Electrical surface properties of nanoporous alumina membranes: influence of nanochannels' curvature, roughness and composition studied via electrokinetic experiments

Ali Vakilinejad, Emmanuelle Dubois, Laurent Michot, Marie Jardat, Didier Lairez, Serge Durand-Vidal, Clément Guibert, Nicolas Jouault

ARTICLE

Electrical surface properties of nanoporous alumina membranes: influence of nanochannels curvature, roughness and composition studied by electrokinetic experiments

Received 00th January 20xx,
Accepted 00th January 20xx

DOI: 10.1039/x0xx00000x

Ali Vakilinejad,[a] Emmanuelle Dubois, [a] Laurent Michot, [a] Marie Jardat, [a] Didier Lairez, [b] Serge Durand-Vidal, [a] Clément Guibert, [c] and Nicolas Jouault *[a]

Among classical nanoporous oxide membranes, anodic aluminum oxide (AAO) membranes, made of non-connected, parallel and ordered nanochannels, are very interesting nanoporous model systems widely used for multiple applications. Since most of these applications involve local phenomena at the nanochannel surface, the fine description of the electrical surface behavior in aqueous solution is thus of primordial interest. Here, we use an original experimental approach combining several electrokinetic techniques (tangential and transverse streaming potential as well as electrophoretic mobility experiments) to measure the ζ-potential and determine the surface isoelectric points (IEPs) of several AAOs having different characteristic sizes and compositions. Using such an approach, all the different surfaces available in AAOs can be probed: outer surfaces (top and bottom planes), pore wall surfaces (i.e., inner surfaces) and surfaces created by the grinding of the AAOs. We find clear IEP differences between the outer, pore wall and grinded surfaces and discuss it in terms of nanochannel and surface morphology (curvature and roughness) and of modifications of the chemical environment of the surface hydroxyl groups. These results highlight the heterogeneities between the different surfaces of these AAO membranes and emphasize the necessity to combine complementary electrokinetic techniques to properly understand the material, approach which can be extended to many nanoporous systems.

Introduction

Because of their unique structural, physical, chemical and surface properties, a wide range of scientific communities now largely employs nanoporous oxide membranes for multiple applications: biosensing[1], nanofiltration[2], nano templating[3], drug delivery[4], catalysis[5], energy storage[6]... Since most of these applications involve local phenomena at the nanochannel surface (adsorption of molecules, chemical reaction…) the fine description of the electrical surface behavior in aqueous solution is thus of primordial interest. For oxides, the existence of an electrical charge is due to the protonation/deprotonation of hydroxyl groups at the surface, which depends on the local chemical environment. The electrical surface properties are usually quantified through the sign and amplitude of the ζ-potential (defined as the electric potential at the hydrodynamic shear plane) and also through the point of zero charge (PZC i.e., pH at which net charge density is zero) or the isoelectric point (IEP i.e., pH at which the ζ-potential is zero) of the materials. PZC is usually obtained by potentiometric titration (which is well adapted for colloidal particles) while IEP is obtained by electrokinetic techniques (streaming current or potential, electrophoresis) more suitable for nanoporous materials (note that IEP and PZC match when there is no specific ion adsorption at the surface)[7]. Electrokinetic data interpretations rely on electrokinetic theories to determine the ζ-potential assuming that the flow at the probed interface is well controlled, implying in particular that the surface is planar, ideal (i.e. smooth), nonporous and rigid (i.e. contrary to "soft"). Any deviations from these hypotheses might modify the relationship between the measured values and the ζ-potential and consequently the IEP of the surface[8, 9].

Among classical nanoporous oxide membranes, anodic aluminum oxide (AAO) membranes are largely used and very interesting nanoporous model systems. Literature survey clearly shows the wide interest of these nanoporous systems for the various applications already mentioned above because of their pore morphology, pore density and surface properties[10]. AAOs are synthesized by a two-step anodization process in an acidic electrolyte that leads to the formation of

[a] Sorbonne Université, Laboratoire PHENIX, CNRS, UMR 8234, 4 place Jussieu, 75005 Paris, France
[b] Laboratoire des Solides Irradiés (LSI), École polytechnique, CNRS, CEA, Institut Polytechnique de Paris, 91128 Palaiseau cedex, France
[c] Sorbonne Université & CNRS, UMR 7197, Laboratoire de Réactivité de Surface (LRS), 4 Place Jussieu, 75252 Paris Cedex 05, France
* Corresponding author: nicolas.jouault@sorbonne-universite.fr
Electronic Supplementary Information (ESI) available: details on the AAO synthesis, additional SEM and AFM images, details on streaming experiments. See DOI: 10.1039/x0xx00000x

non-connected, parallel and ordered nanochannels whose characteristic sizes and composition can be finely tuned through the anodization experimental parameters (voltage, nature and concentration of the electrolyte, temperature…)[11, 12]. Typical nanochannel diameter ranges from 10 nm to 200 nm with a narrow size distribution, the channel length can reach up to 100 µm and the pore density can vary from 10^9 to 10^{11} pores/cm^2, providing selectivity, mechanical stability and interesting high flow rate to AAO membranes. In term of composition, AAOs are heterogeneous: they are made of amorphous alumina (Al_2O_3) with contaminants coming from the electrolyte used during the anodization (for instance oxalate ions when using oxalic acid (OA) or sulfate ions with sulfuric acid). Their quantities mainly depend on the electrolyte concentration and anodization voltage[12]. More precisely, it has been observed that the AAO cell is composed of two regions with different compositions: one contaminants-rich area, the extent of which depends on the contaminant nature (the smaller such as sulfates will diffuse deeper within the cell) and one alumina-rich area. These anion contaminations have impacts on the AAO optical properties (refractive index, photoluminescence) but there were no attempts so far to investigate their effects on the AAO electrical surface properties.

AAO electrical surface properties are primarily investigated by electrokinetic techniques, mostly streaming current or potential measurements. Streaming experiments (SE) can be performed by applying a pressure gradient along the AAO outer surface (tangential SE) or through the AAO nanochannels to probe the inner surface (transverse SE). So far, studies have been carried out on homemade or commercial AAOs using KCl solutions as electrolytes and primarily assuming that both inner and outer surfaces behave similarly, i.e, without combining both transverse and tangential SE. The results show that IEPs range from 6.7 to 7.9 by using tangential SE[13] while higher IEPs are found by transverse SE (from 8 to 10)[14-16]. Moreover, a recent work using electrophoretic mobility (EM) experiments on suspended AAO in KCl solution found lower IEPs of 4.6, 5.3 and 6 for AAOs synthesized in phosphoric, oxalic or sulfuric acid, respectively[17]. In that specific case, the AAOs are grinded to obtain an AAO particle suspension, questioning the effect of such grinding on the nature of the AAO surface probed by EM. Additionally, another technique using electron paramagnetic resonance can also probe the inner surface and lead to the determination of an effective PZC of about 5 for AAOs synthesized under different conditions and with variable pore diameter D_p[18, 19]. For comparison, plain aluminum oxides (including the different crystallographic forms) or aluminum hydroxides (AlOOH and $Al(OH)_3$) have typical IEPs comprised between 8 and 11[20]).

These previous works showed that, depending on the technique used, the type of AAOs and on the nanochannel diameter (D_p), a large range of IEPs is found (from 4.6 to 10), suggesting that the probed surfaces might be different. The origins of these differences can be multiple: *i*) modification in the local chemical environment (coordination[13], density of active sites, chemical surface heterogeneities, preferential adsorption) or *ii*) modification of the structure of the electrical double layer (EDL) induced by surface morphology. For the latter, the influence of curvature or roughness has not been considered for AAO but could also explain the IEP differences[21]. However, with the current results, it is impossible to decorrelate these multiple factors since no systematic studies have been performed to differentiate them on the different surfaces.

In this context, we aim here to investigate the effect of curvature, roughness and composition on the electrical surface properties (ζ-potential and IEP) of AAOs synthesized with three different electrolytes (oxalic acid (OA) with variable concentration, sulfuric acid (Sul) and selenic acid (Sel), both at a fixed concentration of 0.3 M) in order to tune the composition and the diameter D_p of the nanochannels. We will use an original experimental approach combining both tangential and transverse SE on the membranes as well as EM experiments on the grinded membranes to probe all the different surfaces available in AAOs: outer surfaces (top and bottom planes), pore wall surfaces and surfaces created by the grinding of the AAOs. Such approach, never used previously and applied here on AAO membranes, can further help to clarify the electric surface behavior of various systems since it can be used for different types of nanoporous membranes (organic or inorganic).

Experimental

Anodic Aluminum Oxide (AAO) synthesis

Ordered AAOs are synthesized using the classical two-step potentiostatic anodization in acidic electrolyte[11, 22]. First, ultrapure aluminum (Al) foil (between 12 and 25 cm^2, 99.999 % purity, 0.32 mm thick, purchased from Goodfellow) is electropolished under 30 V in a solution made of 20 % vol perchloric acid (70 % from Alfa Aesar) and 80 % vol ethanol (99.8 % from Carlo Erba) during around 40 s at 0 °C. Then, a first anodization is performed during 2 hours in a given acidic electrolyte. Here, three different electrolytes are used: oxalic acid (OA, 99 % from Aldrich), sulfuric acid (95-97 %, Merck) or selenic acid (40 % wt from Aldrich). The concentration of sulfuric and selenic acid solutions is kept constant to 0.3 M while OA concentration is varied (0.8 M, 0.3 M and 0.05 M). Anodization is carried out at a constant voltage and temperature that depends on the nature of the electrolyte used: 40 V / 18 °C, 25 V / 18 °C and 45 V / 10 °C for OA, sulfuric acid and selenic acid, respectively. Then, the formed aluminum oxide is immersed in a phosphochromic acid solution (1.8 wt% CrO_3 and 6 wt% H_3PO_4) at 50 °C with stirring for 2 h in order to be fully dissolved. After this dissolution, the surface of the remaining Al foil keeps the imprints of the dissolved pores from which the second anodization is initiated to ensure good channel ordering[11]. The second anodization is performed under the same conditions (nature of the electrolyte and voltage) as the 1st anodization. The current density *j* (between 1 and 7 mA.cm^{-2}, see Table S1), recorded by a Keithley digital multimeter, depends on the experimental anodization

parameters and drives the AAO growth rate (GR). The final AAO thickness is governed by the interplay between these different parameters and the durations of the 2nd anodization are thus adapted to reach the

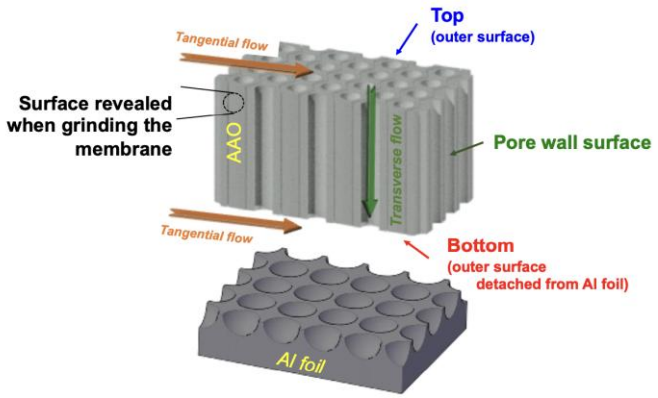

Scheme 1. Schematic representation of the AAO membrane obtained after detachment from the Al foil. The different surfaces investigated by electrokinetic experiments are shown (top and bottom outer surfaces, pore wall surface and surface created after the grinding).

desired AAO thickness (here thickness varies from around 15 to 46 µm).

Finally, a detachment step, described elsewhere[23], is necessary to obtain open-through AAO membranes. Briefly, a 3rd anodization is carried out in a very concentrated sulfuric acid solution (≈ 13 M) under a voltage identical to the previous anodization steps at low temperature (around -1 °C) in order to produce a highly soluble layer of about 3 µm thick. The AAO detachment from the Al surface occurs after dissolution of this layer by etching in the phosphochromic acid solution at 30 °C for a variable duration depending on the type of AAO produced. All the different anodization and detachment conditions used in this work are fully summarized in Table S1 in SI. Finally, after the synthesis, an open through AAO membrane is obtained and different surfaces can be investigated (see Scheme 1): two outer surfaces called top and bottom (the bottom surface being the side that faced the Al foil before detachment) and the pore wall nanochannel surface. In the following, the AAO membranes will be named according to the nature and concentration of electrolyte used (i.e. electrolyte-concentration as for instance OA-0.3 for oxalic acid at 0.3 M).

Scanning Electron Microscopy (SEM) and Energy Dissipative Spectroscopy (EDS)

The AAO morphology (pore diameter D_p, interpore distance D_{int}, channel length L_p and porosity P) is obtained by using Scanning Electron Microscopy (SEM). Sample imaging is performed on a field emission gun SEM (FEGSEM, SU-70 Hitachi) at a low accelerating voltage of 3 kV to avoid charging effects. Images with different magnifications (x50 000 and x100 000) were recorded for the top, bottom and section surfaces and analyzed by ImageJ software after image binarization. A typical image analysis involves about 100 pores for top and bottom surface image and about 20 pores for section image. Additionally, X-ray Energy Dissipative Spectroscopy (EDS) measurements were performed with an OXFORD X-Max SDD at 5 keV to determine the AAO elemental composition (C, O, Al, P, S, Se) after calibration with silicon standard. The amount of C coming from external contamination (i.e, not coming from the anion incorporation) has been estimated by measuring the C / Al content of AAO membranes in which no C due to the anion contamination are expected (on Sul-0.3 and Sel-0.3). The value of C / Al of 0.024 +/- 0.013 was thus found and then subtracted to the C / Al measured for OA AAOs. No S or Se external contaminations have been measured, as observed previously[24].

Atomic Force Microscopy (AFM)

AFM was used to quantify the surface roughness of the outer surfaces. Small pieces of AAO membranes are placed on a double-sided tape put on a circular disk. Images were recorded in Tapping Mode (TM®-AFM) using a Nanoscope III multimode scanning probe microscope (Digital Instruments). In Tapping Mode, the cantilever oscillates at its resonance frequency (typically 200-400 Hz in air), so that the tip interacts very briefly with the surface during each oscillation cycle with a small amplitude (A ~ 10 nm). The reduction of the cantilever oscillation from its set point value, due to interactions between the AFM tip and the sample during the scan, is used to determine the topography of the surface. To minimize the forces of interaction, the ratio of the set point value to the free amplitude of the cantilever was maintained at approximately 0.9 by adjusting the vertical position of the sample. Images were recorded with a resolution of 512 × 512 pixels and a scan rate of 0.5-0.8 Hz. Then, the surfaces roughnesses of AAO membranes were characterized by means of the root mean square (RMS) R_q, which is the root mean square average of height deviations taken from the mean plane.

Fourier Transform Infrared (FTIR) and Attenuated Total Reflection (ATR) spectroscopy

Fourier-transform infrared (FTIR) spectroscopy in transmission mode was conducted on AAO membranes using a FTIR spectrometer (Tensor27, Bruker) with a homemade sample holder that hangs the sample in the IR beam. Background and sample spectra were recorded under air atmosphere with 32 scans. Additionally, ATR infrared spectroscopy was performed using a Thermo Scientific Nicolet iS20 equipped with Smart iTX accessory. AAO membranes were directly put on top of the diamond and spectra were measured with 64 scans for the top and the bottom surface. In ATR mode, the penetration depth depends on the wavenumber: from 100 nm for 4000 cm^{-1} to 1000 nm for 400 cm^{-1}, respectively.

Streaming potential (SP) and streaming current (SC) experiments

In contact with aqueous electrolyte solution the AAO hydroxyl surface groups undergo protonation/deprotonation processes generating surface charges that are compensated by

the presence of ions in solution to ensure electroneutrality. An electrical double layer (EDL), consisting of an immobile Stern layer and a mobile diffuse layer, is formed adjacent to the charged surface. When a pressure gradient is applied, the ions in the diffuse layer are displaced with the fluid and an electrical streaming current (I_s) arises and is associated to an electrical streaming potential (U_s)[9]. Assuming that the surface conductivity is negligible and the ζ-potential of the surface is low, the latter can be expressed as a function of the variation of I_s with pressure difference (eq. 1) or by using the variation of U_s with pressure difference (eq. 2):

$$\zeta = -\frac{\eta}{\epsilon_r \epsilon_0}\frac{1}{\Lambda}\frac{dI_S}{dP} \qquad (1)$$

$$\zeta = \frac{\sigma\eta}{\epsilon_r \epsilon_0}\frac{dU_S}{dP} \qquad (2)$$

$1 / \Lambda$ is the apparatus characteristic length which depends on the channel geometry; σ is the conductivity of the electrolyte solution; η is the viscosity of the electrolyte solution and is assumed to be the same as water; ε_r is the relative permittivity of the electrolyte solution that is also approximated to be the same as water, and ε_0 is the vacuum permittivity. Thus, the measurement of the variation of I_s or U_s with the pressure difference directly yields the ζ-potential of the probed surface.

Here, two different experimental modes with different channel geometries were used to measure I_s and/or U_s. Streaming experiments (SE) are either performed by applying a pressure gradient along the AAO top or bottom outer surfaces (tangential mode) or through the AAO nanochannels to probe the pore wall surface (transverse mode). Both modes are schematically represented in Scheme 1.

1) **Tangential SE** are carried out at room temperature with a SurPASS instrument (Anton Paar GmbH). In this mode, the channel geometry is made of two identical AAO pieces (S = 1 cm x 1 cm) facing each other with a variable and tunable gap distance *h*. The two AAO pieces were mounted with double-adhesive tape on the two surfaces of the SurPASS adjustable-gap cell. The surfaces gap distance *h* is determined by flow measurements using the Hagen-Poiseuille formula and adjusted by a micrometric screw. In all our tangential SE, in order to ensure the establishment of a laminar flow, the typical gap distance is fixed at an average value of 89 +/- 7 µm. The electrolyte solution is circulated back and forth through the cell with two syringe pumps. pH and conductivity are continuously monitored. All experiments are carried out with 100 mM KCl solution, setting the solution conductivity to 12.2 mS/cm and corresponding to a Debye length κ^{-1} of about 1 nm (fulfilling the conditions to apply eq. 1 and 2). The pH of the electrolyte solution is modified by adding small amounts of concentrated HCl or KOH solutions. A pair of Ag / AgCl electrodes is used to measure both I_s and U_s and four streaming measurements are performed (corresponding to two "back and forth" measurements). A typical set of raw data (I_s versus P) is shown in Fig. S1. The ζ-potential obtained by I_s or U_s are similar (see Fig. S2). The AAO membranes are first measured in KCl solution at pH ≃ 6 and the ζ-potential is negative. To ensure that the AAO surfaces are not contaminated by impurities, the pH is thus directly adjusted to a high value (pH around 10) and then decreased stepwise down to about 3 and the ζ-potential is measured for each pH.

2) **Transverse SE** are performed at room temperature with a homemade device composed of two compartments filled with 100 mM KCl solution separated by the AAO membrane (note that in this mode the probed surface is directly the pore wall nanochannel surface). An Ag / AgCl electrode is immersed in each compartment to measure U_s and the pressure is alternatively applied from one compartment to another by solenoid valves with a given frequency of 0.2 Hz. One measurement consists of a "back and forth" cycle of 5 s (see Fig. S3) from which dU_s/dP is extracted and then converted into ζ-potential according to eq. 2. The first measurement is also performed in pure KCl solution and here a positive ζ-potential is measured. As the tangential SE, the pH is then adjusted to high value and followed by stepwise pH lowering down to around 3. For each pH, the cycle is repeated between 10 min and 1 h to obtain an average ζ-potential (see Fig. S4).

Electrophoretic mobility (EM) experiments

Electrophoretic mobility (EM) measurements are performed using the ZetaSizer NanoZS (Malvern Instruments) at 20 °C following the same pH variation cycle as the SP experiments. As previously, the pH is adjusted by adding small volumes of concentrated KOH or HCl solutions and is measured before and after the EM measurements. Once the pH is stable, three measurements made of three runs are performed for each pH value to obtain an average ζ-potential.

EM measurements can provide the ζ-potential value of AAO when the sample is formulated as particles suspended in aqueous solution. To obtain AAO particles, about 1 mg of AAO membrane are grinded manually in a mortar and further dispersed in 2 mL of 100 mM KCl solution. The suspensions are not stable in time, indicating a large distribution of particle sizes, the biggest ones sedimenting rapidly. The volume size distribution of the AAO particles in solution is thus determined by combining complementary techniques. First, laser granulometry that can provide sizes from the microns up to few millimetres is performed using the Mastersizer 3000 (Malvern Instruments) on the suspension under a constant stirring of 500 rpm. Additionally, Dynamic Light Scattering (DLS) has been performed with a Vasco KIN (Cordouan Technologies, laser wavelength of 638 nm with a detection angle of 170°) on a suspension without stirring in which bigger objects will sediment with time making the sizes of smaller objects measurable. Finally, SEM has also been conducted on the grinded AAO powder deposited on a carbon tape.

Results and discussion

Structure and composition of AAO membranes

The final structural morphology (pore diameter D_p, interpore distance D_{int}, length L_p, pore density) and composition of AAO membranes are a consequence of a complex interplay between different experimental parameters used during the anodization: voltage, temperature, nature and concentration of the electrolyte and anodizing time. Thus, by varying these parameters, one can tune the AAO structure and composition to further investigate their influence on the AAO electrical surface properties, an important issue we wish to address here.

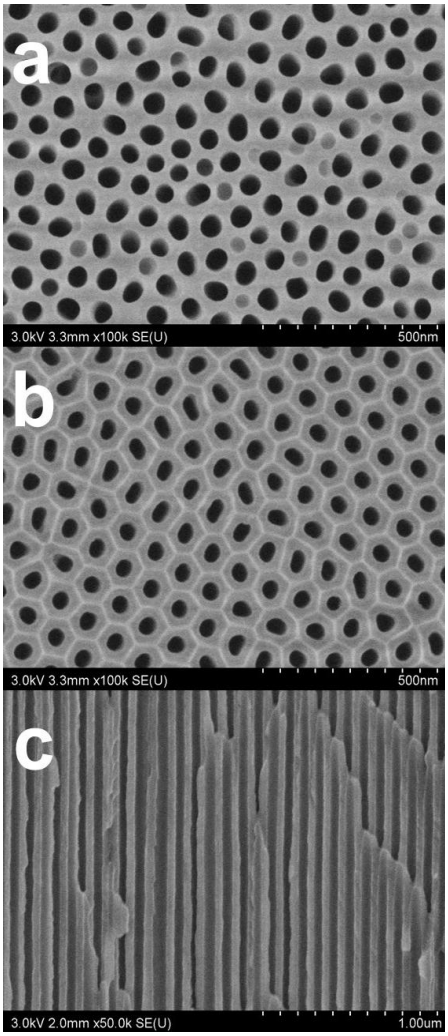

Figure 1. SEM images of the OA-0.8 AAO membrane of a) the top surface b) the bottom surface and c) from the section view.

Fig. 1a and 1b show typical SEM images of AAO membrane prepared with 0.8 M OA (named OA-0.8). Image analysis of the top and bottom surfaces yields pore diameters D_p of 55 +/- 5 nm and 47 +/- 4 nm, respectively. The difference in size between the top and the bottom (around 15 %) is due to the longer exposure of the top surface to the acidic electrolytes during the synthesis that enlarges the top D_p (such small variation in D_p is similar to what has already been observed in the literature[23]). Analysis of the section image (Fig. 1c) yields a D_p of 46 +/- 5 nm closer to the bottom one, indicating that the bottom pore diameter is more representative of that along the nanochannel. This section view also clearly shows that the nanochannels are straight and non-connected over several microns and thus AAOs can be considered as a collection of individual infinitely long nanochannels (since $D_p << L_p$) in contrast to nanopores ($D_p \approx L_p$), which is an important approximation for the analysis of electrokinetic experiments[25].

AAO membranes have also been synthesized by using lower OA concentrations (0.3 M and 0.05 M) while keeping the voltage and temperature unchanged (40 V and around 18 °C, respectively). Thus, by only reducing the OA concentration, one expects marginal changes in pore diameter D_p.

Sample	D_p (nm)		L_p (μm)
	Top	Bottom	
OA-0.05	61 ± 8	53 ± 8	15.9
OA-0.3	53 ± 5	46 ± 4	19.5
OA-0.8	55 ± 5	47 ± 4	24.3
Sul-0.3 (1)	47 ± 3	31 ± 2	38.3
Sul-0.3 (2)	47 ± 3	27 ± 2	46.3
Sel-0.3	53 ± 3	43 ± 2	20.2

Table 1. Characteristics pore diameters and lengths measured by SEM analysis for the AAOs membranes.

The corresponding structural parameters obtained by SEM analysis are shown in Table 1. The bottom value of D_p is similar for 0.3 M (46 +/- 4 nm) and slightly higher for 0.05 M (53 +/- 8 nm). Note that, for a given electrolyte and temperature, the pore D_p is mostly influenced by the voltage[26]. Hence, as expected, here the OA concentration has a limited influence on D_p.

In addition to OA, AAO membranes have also been synthesized by using two other electrolytes such as sulfuric acid or selenic acid, at a similar concentration as OA-0.3 (details of the synthesis with the experimental parameters are shown in Table S1). Fig. S5 shows the corresponding SEM images of Sul-0.3 and Sel-0.3 and Table 1 presents the structural parameters obtained from the image analysis. For Sul-0.3 the bottom value of D_p drops down to an average value of 29 +/- 3 nm, i.e, a decrease of 37 % compared to OA-0.3, while it remains almost similar for Sel-0.3 (43 +/- 2 nm).

In terms of composition, as mentioned in the introduction, AAOs are made of amorphous alumina (Al_2O_3) containing additional elements (C, S, Se) coming from the electrolyte used during the anodization and it has been shown that the atomic ratio between these elements and Al increases with the average current density <j>[27]. By using OA, oxalates are incorporated within the bulk AAO. Their amount mainly depends on the OA concentration (at a given voltage) and can be quantified by elemental analysis of the carbon (C) content with EDS. Since EDS has a typical penetration depth of about 400 nm such analysis provides information about the bulk AAO composition and can be performed on the top, bottom and

section surfaces of the AAO (see Scheme 1). Fig. 2a shows the evolution of C / Al atomic ratio as a function of <j> for AAOs membranes produced with OA at different concentrations. For each condition, no significant differences are measured between the top, bottom and sections surfaces. For OA-0.8 membrane, the ratio C / Al reaches a value of about 0.08 for the top, bottom and sections surfaces and decreases down to 0.025 when the OA concentration decreases (i.e, decreases when the value of <j> decreases). Thus, less oxalates are incorporated within the AAO bulk by using OA electrolyte at lower concentrations.

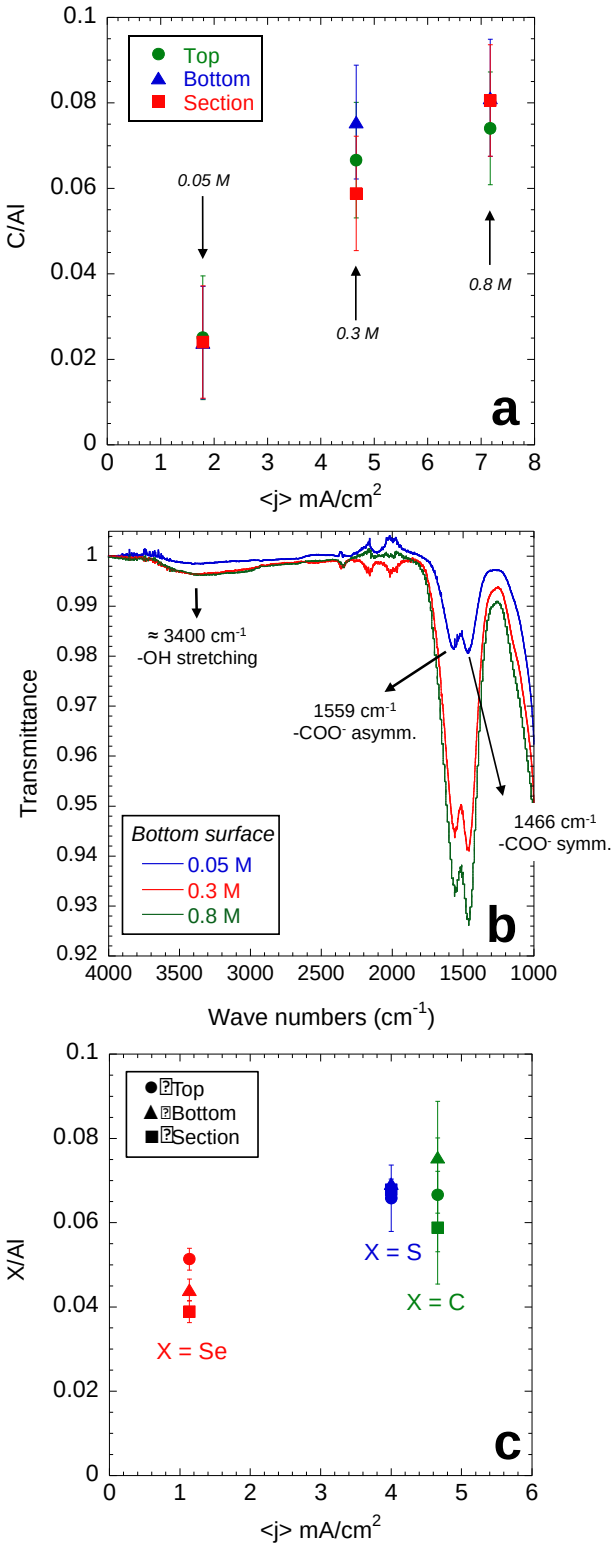

Figure 2. a) Atomic ratio C / Al obtained from EDS as a function of average anodization current density (< j > in mA/cm^2) of AAO membranes synthesized with different OA concentrations (0.05 M, 0.3 M and 0.8 M) for top (circle), bottom (triangle) and section (square) surfaces. b) Infrared spectra in ATR mode made on the bottom surface of OA AAO membranes (0.05 M, 0.3 M and 0.8 M). c) X over Al ratio as a function of < j > for OA-0.3 (green), Sul-0.3 (blue) and Sel-0.3 (red) AAO membranes: top (circle), bottom (triangle) and section (square) surfaces.

Complementary ATR infrared measurements made on both the top and bottom surfaces (see Fig. 2b for the bottom surface) show that the amplitude of the double bands related to the carboxylates O-C=O groups of the oxalates (symmetric and asymmetric stretching vibrations at 1466 cm^{-1} and 1559 cm^{-1}, respectively) increases with the OA concentration, in agreement with the EDS trend. Additionally, the bands separation Δν (= 93 cm^{-1}), similar for all OA AAO membranes, indicates a bidentate Al-oxalate coordination[28]. Thus, changing the amount of oxalates within the AAO does not modify the local Al environment, as confirmed recently by the determination of the Al-O average coordination number by ^{27}Al NMR spectroscopy that was estimated as being about 4.75 independently of the oxalates contents[29].

By changing the nature of electrolyte, the nature of the incorporated anions changes: sulfates or selenates for sulfuric or selenic acid, respectively. Fig. 2c shows the X / Al ratio (X being C, S or Se) obtained by EDS for AAO membranes produced with OA, sulfuric or selenic acids at 0.3 M as a function of the average current density <j>. Indeed, by changing the nature of electrolyte, the value of <j> is modified and accordingly the level of anion incorporation within the AAOs. Interestingly, here, the OA-0.3 and Sul-0.3 have close < j > and thus similar S / Al and C / Al (about 0.07). On the contrary, the Se content in Sel-0.3 AAO is lower (= 0.04 – 0.05), presumably due to the lower value of <j>.

To summarize, the AAO pore diameter and composition can be tuned by controlling the different experimental parameters during synthesis, which is beneficial for independently studying the effect of pore diameter and composition on AAO electrical surface properties. We can decorrelate them by comparing the different samples in order to *i*) study the effect of contaminants amount at constant diameter D_p, *ii*) study the effect of the electrolyte nature at constant contaminants amount and constant D_p, *iii*) study the effect of D_p at constant contaminants amount. In the following, the AAO electrical surface properties are investigated by combining several electrokinetic experiments to probe all the AAO surfaces: tangential SE for the top and bottom outer surfaces, transverse SE for the pore wall nanochannel surface and EM for surfaces created after the AAO grinding (see Scheme 1).

Electrical surface properties of AAO membranes

Isoelectric points (IEPs) of the different probed surfaces: outer, pore wall and grinded surfaces.

Fig. 3 shows the evolution of ζ-potential as a function of pH for OA-0.8 AAO membrane measured by transverse SE, tangential SE and EM measurements. From these curves the IEPs of the different probed surfaces, i.e. the pH at which the ζ-potential is zero, can be determined. The following values of IEP of 6.7, 6.9, 9.8 and 5.1 can be determined for outer top, outer bottom, pore wall and grinded surfaces, respectively. The transition from positive to negative is smooth for tangential SE measurements while it is sharp for EM. Also, the positive and negative ζ-potentials have similar absolute value for both cases (between 20 - 25 mV).

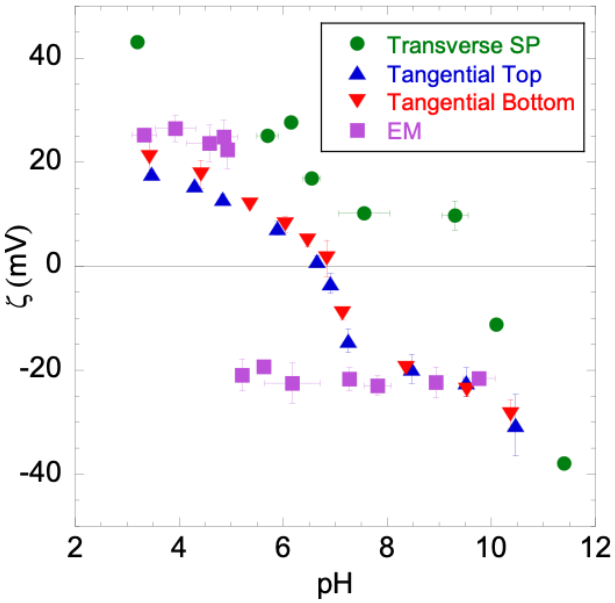

Figure 3. ζ-potential evolution as a function of pH for OA-0.8 AAO membrane measured by transverse SP (green circles), by tangential SC on the top (blue triangles) and bottom (red triangles) surfaces, and by electrophoretic mobility (EM) on the grinded AAO (purple squares).

For transverse SE, the transition is also smooth but it displays higher absolute ζ-potential values (up to 40 - 45 mV) and the negative plateau is not reached over the investigated pH range because of the high IEP. Besides, The top and the bottom outer surfaces present a similar IEP (≈ 7), which is quite different from the pore wall surface (= 9.8) and the grinded surface (= 5.1). Thus, a clear change in IEPs (above 1 pH unit) is observed depending on the probed surface: $IEP_{grinded} < IEP_{outer} < IEP_{inner}$. In the following, we propose to investigate the possible origins of the difference between the IEPs by decoupling the various effects of the different synthesis parameters that have been described above.

Influence of the amount and nature of "contaminants" within AAOs.

Let us first focus on the effect of contaminants (oxalates) content. As mentioned previously, by changing the OA concentration, AAOs present similar diameters D_p (13 % difference) but large variations in oxalates content (from 0.08 to 0.025, above 70 % difference), especially between 0.05 M and 0.8 M. Fig. 4 shows the evolution the ζ-potential as a function of pH for OA-0.05, OA-0.3 and OA-0.8 AAO membranes for the top outer (Fig. 4a) and bottom outer surfaces (Fig. 4b), the pore wall surface (Fig. 4c) and the grinded surface (Fig. 4d) whereas Table 2 provides the corresponding IEP values. Small variations (< 1 pH unit) are observed for the outer (tangential top and bottom) and pore wall (transverse) surfaces when changing the oxalates amount:

IEPs range from 6.4 to 7.1, from 6.1 to 6.9 and from 9.2 to 9.8 for the top, bottom and pore wall surfaces, respectively.

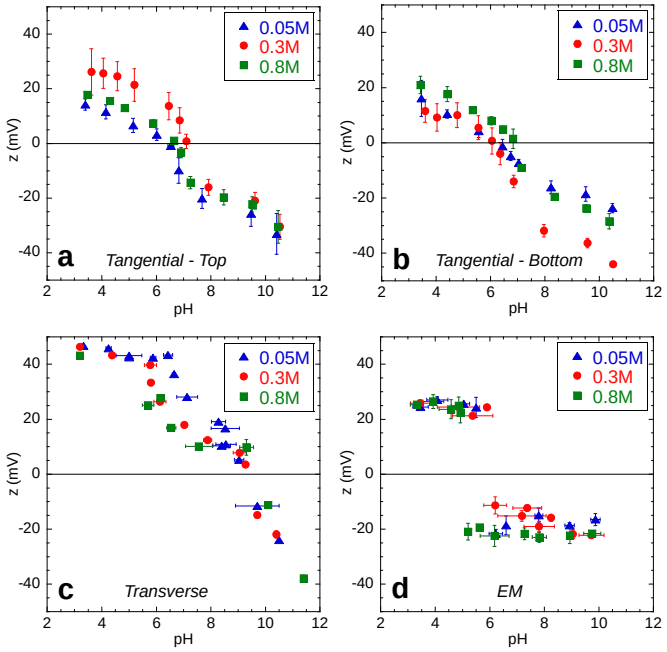

Figure 4. ζ-potential evolution as a function of pH for OA-0.05 (blue triangles), OA-0.3 (red circles) and OA-0.8 (green squares) AAO membranes synthesized in oxalic acid solution at different concentrations measured by **a)** tangential SC on top and **b)** bottom surfaces, **c)** by transverse SP and by **d)** electrophoretic mobility (EM) of the grinded AAO membranes.

For EM, since the transition is sharp, the uncertainties in IEP determination are lower and an IEP increase of 1 pH unit (from 5.1 to 6.1) is observed by decreasing the OA from 0.8 M to 0.3 M but remains unchanged by decreasing further the OA concentration down to 0.05 M. Since the C/Al content decreases less between 0.8 M and 0.3 M than between 0.3 M and 0.05 M, the IEP modification is not proportional to the oxalate content. The specific case of EM data will be discussed in a dedicated section below.

Table 2. IEP of the studied membranes obtained from the ζ-potential measurements by tangential flow streaming current on top and bottom surfaces, transverse flow streaming potential inside the nanochannels and electrophoretic mobility (EM) of the grinded membrane samples. For Sul-0.3 and Sel-0.3 not enough sample from one synthesis were available to perform the full set of SE measurements because of some inherent difficulties encountered during the detachment step detailed in the AAO synthesis section. Thus, for Sul-0.3, experiments were done on AAOs from two different syntheses (denoted (1) and (2)) and, for Sel-0.3, since AAOs pieces were regularly too small, only the tangential SE of the top side was performed.

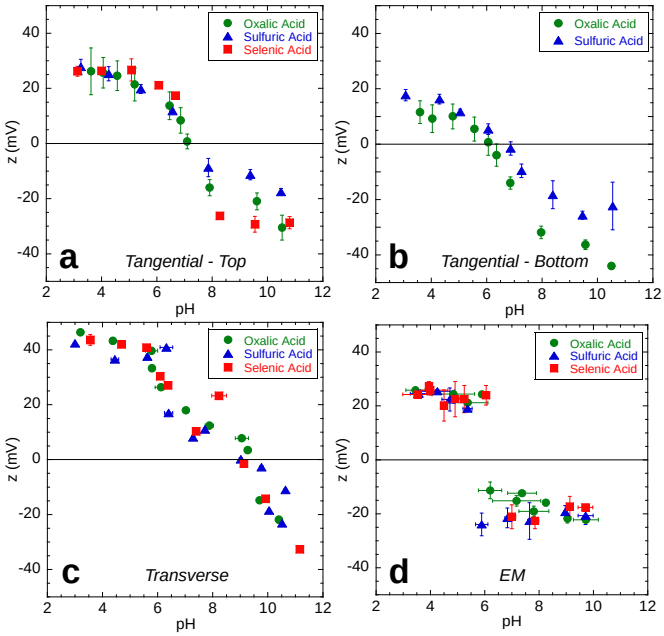

Figure 5. ζ-potential of the OA-0.3, Sul-0.3 and Sel-0.3 membranes synthesized in 0.3 M oxalic, sulfuric and selenic acid solutions and measured by **a)** tangential flow streaming current on the top and **b)** bottom surface, **c)** transverse streaming potential inside the nanochannels and **d)** electrophoretic mobility (EM) of the grinded membrane sample.

Let us focus on the effect of the contaminant nature, which can be modified during synthesis in order to incorporate either sulfates or selenates instead of oxalates. Fig. 5 shows the evolution of the ζ-potential as a function of pH for OA-0.3, Sul-0.3 and Sel-0.3 AAO membranes for the top outer (Fig. 5a), bottom outer surfaces (Fig. 5b), the pore wall surface (Fig. 5c) and the grinded surface (Fig. 5d) and the corresponding IEP values are shown in Table 2. Here again, no drastic changes are measured for the outer, pore wall and grinded surfaces when the nature of contaminants is changed. For instance, OA-0.3 and Sel-0.3 AAO membranes have different contamination natures and amount but similar IEPs. Thus, the surface group properties are not affected by the AAO bulk composition.

Influence of nanochannel curvature.

In addition to the amount and to the nature of contaminants that showed not to affect significantly the IEP, the question of the curvature effect can be raised and explored by changing the diameter D_p of the pores. Indeed, Pedimonte et al measured in tangential mode an increase of IEP with D_p (≈ 1.2 pH unit from a D_p of 15 nm to 40 nm) on

Samples	IEP			
	Top	Bottom	Transverse	EM
OA-0.8	6.7	6.9	9.8	5.1
OA-0.3	7.1	6.1	9.4	6.1
OA-0.05	6.4	6.2	9.2	6.1
Sul-0.3 (1)	-	6.7	9	5.5
Sul-0.3 (2)	7.3	-	-	-
Sel-0.3	7.3	-	9	6

non-detached thin porous alumina films. This shift is proposed to result from the existence of two areas with different Al coordination, the relative proportion of which varies with the size of the pores, assuming a composition independent on the pore sizes [13]. On the contrary, Baca et al. observed no significant variation of the IEP for pores ranging from 2 to 20 nm, however on commercial mesoporous alumina and using classical titrations, as large amounts of samples are available [30].

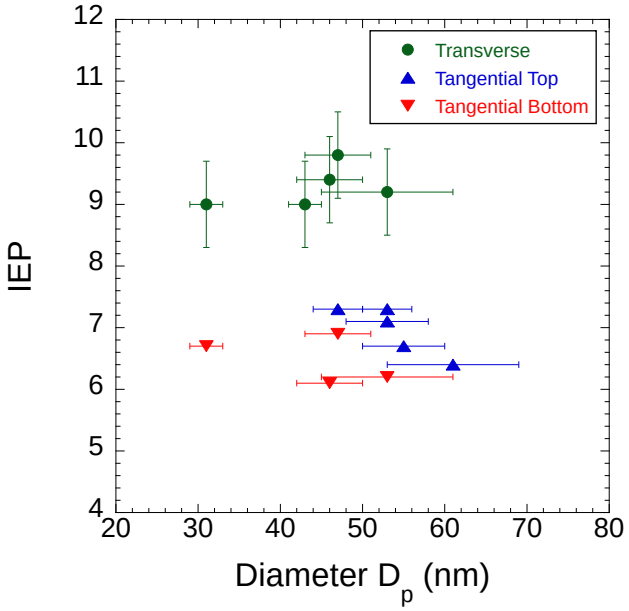

Figure 6. IEP as a function of nanochannel diameters D_p obtained by transverse (green circles) and tangential SE (top: blue triangles; bottom: red inversed triangles). The error bars of the IEPs obtained by transverse SE were estimated from two measurements performed on OA-0.3 AAOs.

This effect of curvature can be analysed from our data on the IEPs determined by tangential and transverse SE since, for EM, AAO is grinded and the probed surfaces are presumably different (see next section below). Fig. 6 displays the IEPs as a function of nanochannel D_p and there is no significant IEP variation with D_p, indicating that, within our investigated range of D_p (from 31 nm to 61 nm), no curvature effect is observed whatever the SE mode used (tangential or transverse), confirming the results of Baca et al [30] with alumina with different pore sizes and similar composition. Note that, as in our case, the ionic strength is such that the diffuse layers are not large enough to overlap so that an effect due to overlap cannot be excluded for lower ionic strengths. Concerning our tangential measurements, they do not show the same trend as Pedimonte et al [13], however the pore diameters D_p are larger in the present study and their variations of IEPs are not so large. Their interpretation is nevertheless connected to the existence of different regions in the material, here probed by the different electrokinetic techniques, enlightening large differences that will be discussed later in the last section.

The case of electrophoretic mobility (EM) measurements

Finally, let us focus on the EM experiments for which different results have been obtained. Contrary to the SE, the AAO is grinded for EM to prepare a particle suspension. Fig. 7a shows the SEM images of the AAO powder after grinding it in a porcelain mortar. Objects with multiple sizes below 100 μm are observed. At higher magnification (Fig. 7b) the porous structure is still visible and the nanochannels are preserved.

ARTICLE

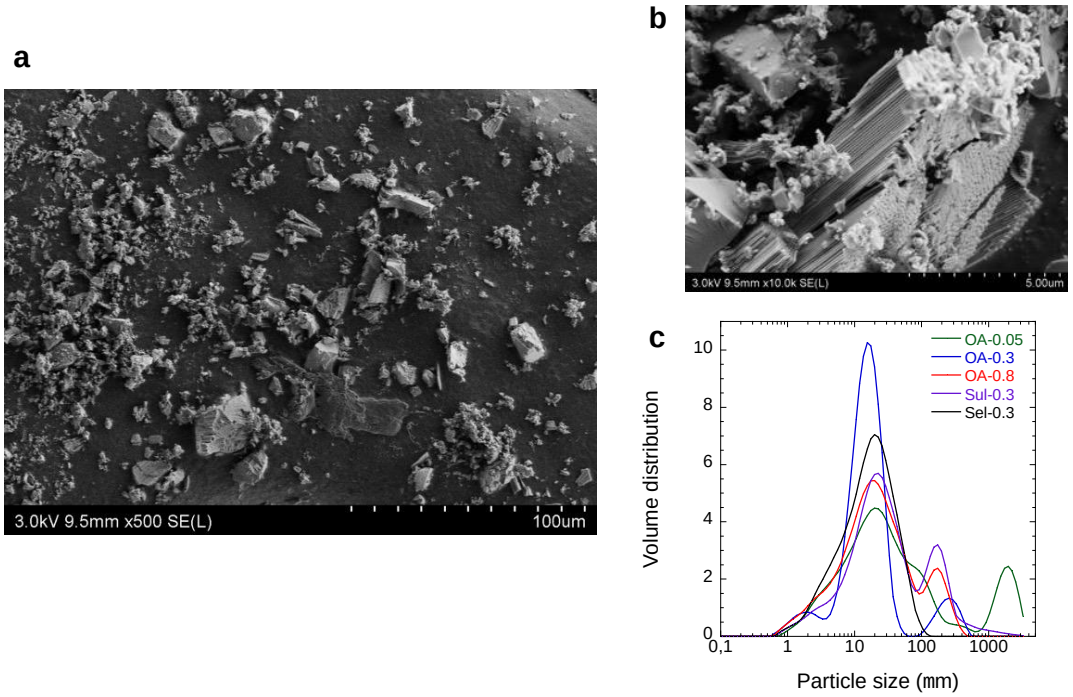

Figure 7. (a) and (b) SEM images of OA-0.8 AAO membrane manually grinded in a porcelain mortar. (c) Volume size distribution as a function of particle diameter obtained by laser granulometry for the different AAO suspensions studied by EM. The volume size distribution is an average of 5 measurements. OA-0.05 also presents larger objects (> 1000 µm) that can be dust since all these solutions are not filtered prior to measurement.

Once the AAO powder is dispersed in aqueous solution, the volume size distribution can be obtained by laser granulometry for the different AAO suspensions studied by EM. Several populations in size are measured for each sample, the highest proportion being centered on 20 µm, value of the order of the membrane thickness (see Fig. 7c), indicating a good reproducibly of the grinding process with the mortar. Additionally, DLS performed on suspensions without stirring revealed that, after sedimentation of the biggest objects (typically after 60 mins), the typical size is around 1 to few microns.

Note that EDS measurements performed on the sample area shown in Fig. 7a reveal the presence of silicon Si, certainly coming from the porcelain mortar and pillar. To rule out the possible influence of Si on the measured IEPs, we also grinded OA-0.8 AAO with an agate mortar (for which no Si has been detected by EDS after grinding) and performed EM and laser granulometry (see Fig. S6). The volume size distribution in Agate is similar in terms of population sizes but with a higher proportion of large objects of about 250 µm (Fig. S6b). However, the evolution of the ζ-potential with pH is similar with the same IEP as the AAO sample grinded with porcelain mortar and pillar (Fig. S6c). The measured IEPs of samples grinded in porcelain mortar are thus not affected by the presence of Si. For our different AAOs, the IEPs obtained by EM finally range between 5.1 and 6.1 (listed in Table 2). They are consistent with recent experiments done on similar AAO crushed membranes[17], and are close to the tangential ones. The main question arising here is about the nature of the probed surfaces during EM. In the membrane, the surface area of the pore walls is around 200 times larger than the outer surfaces (top and bottom). However, the grinding process creates new surfaces, exposing the bulk AAO, i.e. the material located inside the walls that are between the channels. The area of this new surface is at least of the order of the area of the pore walls and can thus modify the IEP of the grinded membranes. The data from Table 2 indicate that the IEP of the new surfaces, which correspond to the material inside the wall, is lower than the IEP of the pore walls. It could be due to the quantity of contaminants incorporated in the material, evidenced with EDS and ATR-FTIR (Fig. 2). Neither the amount of contamination nor its nature (C, S or Se) has a huge impact on the IEPs, which vary by half a pH unit. Additionally, another surprising observation in the EM measurements is the sharp transition between positive and negative ζ-potentials,

suggesting the existence of hydroxyl groups displaying all the exact same pKa value. However, it would be in contradiction with our tangential and transverse streaming experiments and with the literature that shows the existence of different surface hydroxyl sites on the alumina surfaces[31]. This observation could be rationalized by taking into account the fact that EM measurements are performed on AAO powder dispersed in solution, such dispersions sedimenting with time. Indeed, we can hypothesize that particles with lower absolute ζ-potential will presumably quickly aggregate and/or sediment and not be measured by EM, and thus only a fraction of objects with higher absolute ζ-potential remains stable in solution and is probed by EM, displaying then an apparent sharp transition.

Finally, the obvious first conclusion from these measurements is that EM measurements of grinded AAO do not provide an IEP that corresponds to the one of the classical surfaces of the AAOs used in multiple applications in the form of membranes (i.e., pore wall or outer surfaces).

How can we reconcile the tangential and transverse measurements?

This last section is dedicated to the discussion about the clear difference between IEPs determined by tangential (≈ 7) and transverse SE (≈ 9). From the previous sections, we concluded that both SE modes, taken separately, are not influenced by composition or curvature. However, a clear shift is observed between these two SE modes, evidencing differences between the probed surfaces.

Let us recall that the differences are not due to possible external contaminations or AAO chemical transformation in water. For the former, the pH was directly adjusted to a high value (pH ≈ 10) to ensure that, for both SE modes, the AAO surfaces were not contaminated by impurities and then decreased stepwise down to about 3. Moreover, the surfaces obtained after grinding, which cannot be polluted as the others could be, give even lower IEP values, strengthening the existence of a difference depending on the probed surface. For the latter, it has been shown that the chemical transformation is a slow process that can decrease the density of active sites at the surface[32]. Here the experiments duration is typically ranging between 2 h and 9 h to perform a complete ζ-potential versus pH curve, i.e., is shorter than the time needed to initiate the alumina chemical transformation (typically > 1 day), indicating that our surfaces remain stable in term of density of active OH sites within our experimental time window.

As for the possible origins in IEP differences, it can first be noted that probed surfaces are presumably different between the tangential and transverse mode in term of i) surface morphology (roughness) and/or ii) chemical environment (including coordination, density of active sites, or atomic composition). In tangential mode the probed surface consists in an alternance of two types of regions: holes (corresponding to the opening of the nanochannels) and alumina that is also heterogeneous in composition (see Fig. 8a and 8b). In transverse mode the probed surface is only made of alumina homogenous in composition (see Fig. 8c).

The morphology, and in particular the surface roughness, could have an influence on the IEP. Here, the RMS roughness (R_q) of the outer surfaces of OA membranes have been determined by AFM measurements. AFM images are shown in Fig. S7 and the results are presented in Table 3. R_q ranges from 7 nm to 17.5 nm and increases when D_p increases (OA-0.05 > OA-0.3 > OA-0.8). For a given AAO, no differences are observed between the top and bottom surfaces.

On the contrary, the roughness of the inner surface is more challenging to probe. By using SAXS, Engel et al. found a roughness of 0.5 nm[33], significantly smaller than the outer surfaces. Thus, both probed surfaces have clear roughness difference.

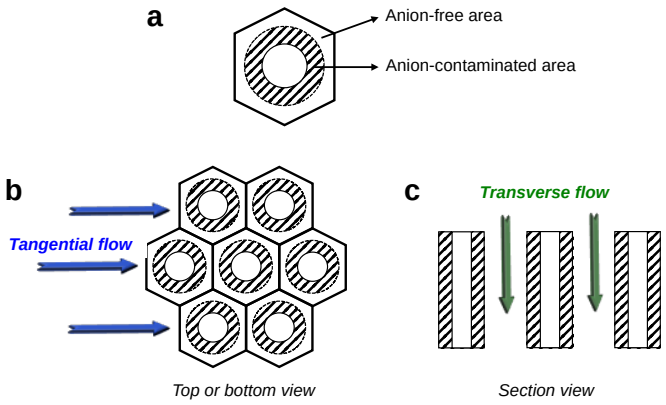

Figure 8. (a) Schematic representation of AAO hexagonal cell made of two areas: one anion contaminated (hatched region) and one anion-free. (b) Top or bottom schematic representation of the outer surface exposed to the tangential flow. (c) Section view with the exposed AAO surface to the transverse flow.

The influence of roughness on IEP has been studied by Borghi et al.[21] on non-porous TiO_2 films of various roughnesses (4 to 26 nm) using AFM force measurements with a colloidal probe in 1 mM NaCl solution, giving a Debye length of 9.6 nm i.e, in the middle of the roughness range. The IEP decreases by 3 pH units between the flattest and the roughest surfaces and the authors propose that this shift originates from the diffuse layer overlap. In our case, the Debye length is much smaller (1 nm) compared to the estimated roughness but we cannot fully exclude that some roughness on the same scale modifies the IEP compared with the one of the very smooth pore surface. Additionally, in these conditions where the Debye length is smaller than the roughness dimension, a decrease of the ζ-potential due to the shear flow attenuation by the protrusions is expected [8] and it can explain the decrease in absolute ζ-potential compared to the inner surface we observed (Fig. 3).

Let us explore now the possibility of IEP shift due to the modification of local chemical environment: coordination, density of active sites, atomic composition or preferential adsorption. It has been repeatedly evidenced that AAO are

AAO membrane	R_q (nm)	
	TOP	BOTTOM
OA-0.05	15.7 +/- 3.2	17.5 +/- 2.2
OA-0.3	10.6 +/- 0.5	9.9 +/- 1.5
OA-0.8	7.0 +/- 1.1	6.9 +/- 1.7

Table 3. RMS roughness R_q determined by AFM measurements. The corresponding images are shown in SI (see Fig. S7).

heterogeneous in composition (Fig. 8a) with an anion contaminated and anion-free area. The extent of the anion-contaminated region depends on the nature and on the size of the contaminants: the smaller the contaminant, the more extended the contaminated area[12]. Discriminating between the two regions is rather difficult as direct measurements like XPS can only probe the surface atomic composition of the whole outer surfaces and the inner pore wall surface is not directly available. However, due to this heterogeneity, as shown in Fig. 8, the tangential SE probes a heterogeneous surface while the transverse mode only probes a homogeneous anion-contaminated area.

The IEP shift could be then interpreted as the consequence of the differences in the chemical environment of the surface hydroxyl groups. The protonation / deprotonation process of the OH groups is sensitive to heterogeneities at the surface and the dissociative constant (i.e. pKa's) can differ from each other because of the number of surrounding Al^{3+} (i.e. singly, doubly or triply coordinated OH groups) and/or by the Al^{3+} coordination number (CN)[31]. The average CN was estimated by ^{27}Al NMR around 4.75 with a predominance of 5-fold coordinated Al for AAOs synthesized in OA, sulfuric or phosphoric acid[29]. Additionally, Ijima et al. proposed by using ^{27}Al NMR that the anion-contaminated area is mainly composed of 6-fold coordinated Al^{3+}, while the anion-free area is composed of 4-fold and 5-fold coordinated Al^{3+}[34]. It was reported that single OH within a 6-fold coordinated Al^{3+} has a pKa of 9.5 while it was 4.4 for single OH within 4-fold coordinated Al^{3+}[31]. These observations allow us to propose an interpretation to reconcile the observed IEP differences between outer and inner surfaces. The inner surface (that corresponds to the anion-contaminated area) might be composed of single OH within a 6-fold coordinated Al^{3+} with a pKa of 9.5, consistent with our IEP of around 9. On the other hand, the outer surfaces, as well as the surfaces probed after grinding (which are made of both anion-contaminated and anion-free regions) might be composed of both OH types (pKa of 9.5 and 4.4) and can yield an average IEP of 6 – 7 depending on the proportions of both types. A similar argument has been used by Pedimonte et al. to explain the IEP shift observed for the top outer surface with tangential SE[13]. Their interpretation is however different: they consider singly coordinated Al-OH (with 2 pKa giving a predicted IEP of 8.5) on the flat area (corresponding to the anion-free region) and doubly coordinated Al_2-OH, also with 2 pKa giving a predicted IEP of 5.4, on the curved area around the channel aperture (corresponding to the anion-contaminated region). Changing the pore diameter modifies the proportion of these two areas and therefore the IEP. Although the depth of contamination depends on the synthesis conditions, this contamination should be higher in the curved area at the top of the pores than in the flat area between the pores, which means that their conclusion is opposite to our results. However, the direct study of the inner pore wall surface and of the grinded material and the decoupling of the different parameters that can change in these nanoporous materials strengthen the result of a higher IEP on the anion-contaminated areas.

Conclusions

The electrical surface properties of AAO membranes have been studied by combining several electrokinetic techniques in order to determine the surface ζ-potential and IEPs. By using tangential and transverse streaming potential/current as well as electrophoretic mobility (EM) experiments, the outer (top and bottom planes), the pore wall surfaces and the surfaces created after grinding can be probed. Interestingly, a clear IEP difference of about 2 pH unit is measured between the outer and the pore wall surfaces, which means that the outer and pore wall surfaces can be of opposite sign on a range of pH. This difference can be attributed to a modification of the local chemical environment of surface hydroxyl groups, i.e., the number of surrounding Al^{3+} and/or the Al^{3+} coordination number. Additionally, the IEPs obtained by EM on grinded membranes are also clearly different from the pore wall surfaces and are slightly lower than the ones of the outer surfaces. The grinding process creates new surfaces, exposing the materials of the AAO walls, the composition of which depends on the nature and amounts of contaminants. This work shows that the electrical surface properties of a single nanoporous material can differ depending on the nature of the probed surface and that only complementary electrokinetic experiments can provide unambiguous interpretations of AAO surface behavior. Finally, our experimental approach can further help to clarify the electric surface behavior of various systems since it can be used for different types of nanoporous membranes (organic or inorganic).

Conflicts of interest

There are no conflicts to declare.

Acknowledgements

David Montero is gratefully acknowledged for conducting SEM and EDS experiments. SEM and EDS were funded by Sorbonne Université, CNRS and Région Ile de France, and are part of FCMat, the Federation of Chemistry and Materials of Paris-Center.

References

1. G. Rajeev, B. Prieto Simon, L. F. Marsal and N. H. Voelcker, *Advanced Healthcare Materials*, 2018, **7**, 1700904.
2. I. Sadeghi, P. Kaner and A. Asatekin, *Chemistry of Materials*, 2018, **30**, 7328-7354.
3. C. T. Sousa, D. C. Leitao, M. P. Proenca, J. Ventura, A. M. Pereira and J. P. Araujo, *Applied Physics Reviews*, 2014, **1**, 031102.
4. M. Szuwarzyński, L. Zaraska, G. D. Sulka and S. Zapotoczny, *Chemistry of Materials*, 2013, **25**, 514-520.
5. D. M. Dotzauer, J. Dai, L. Sun and M. L. Bruening, *Nano Letters*, 2006, **6**, 2268-2272.
6. P. Banerjee, I. Perez, L. Henn-Lecordier, S. B. Lee and G. W. Rubloff, *Nature Nanotechnology*, 2009, **4**, 292-296.
7. J. Lyklema, *Fundamentals of Interface and Colloid Science: Part II Solid-Fluid Interfaces*, Academic Press, London, 1995.
8. M. Zembala, *Advances in colloid and interface science*, 2004, **112**, 59-92.
9. A. V. Delgado, F. González-Caballero, R. J. Hunter, L. K. Koopal and J. Lyklema, *Journal of Colloid and Interface Science*, 2007, **309**, 194-224.
10. A. Ruiz-Clavijo, O. Caballero-Calero and M. S. Martín-González, *Nanoscale*, 2021.
11. H. Masuda and K. Fukuda, *Science*, 1995, **268**, 1466-1468.
12. W. Lee and S. J. Park, *Chemical Reviews*, 2014, **114**, 7487-7556.
13. B. J. Pedimonte, T. Moest, T. Luxbacher, C. von Wilmowsky, T. Fey, K. A. Schlegel and P. Greil, *Acta biomaterialia*, 2014, **10**, 968-974.
14. A. Szymczyk, P. Fievet, B. Aoubiza, C. Simon and J. Pagetti, *Journal of Membrane Science*, 1999, **161**, 275-285.
15. B. H. Winkler and R. E. Baltus, *Journal of Membrane Science*, 2003, **226**, 75-84.
16. A. Christoulaki, D. Lairez, E. Dubois and N. Jouault, *ACS Macro Letters*, 2020, **9**, 794-798.
17. J. Wang, C. S. Law, S. Gunenthiran, H. N. Que Tran, K. N. Tran, S. Y. Lim, A. D. Abell and A. Santos, *ACS Applied Materials & Interfaces*, 2022.
18. E. G. Kovaleva, L. S. Molochnikov, U. Venkatesan, A. Marek, D. P. Stepanova, K. V. Kozhikhova, M. A. Mironov and A. I. Smirnov, *The Journal of Physical Chemistry C*, 2016, **120**, 2703-2711.
19. E. G. Kovaleva, L. S. Molochnikov, D. Tambasova, A. Marek, M. Chestnut, V. A. Osipova, D. O. Antonov, I. A. Kirilyuk and A. I. Smirnov, *Journal of Membrane Science*, 2020, **604**, 118084.
20. M. Kosmulski, *Advances in Colloid and Interface Science*, 2016, **238**, 1-61.
21. F. Borghi, V. Vyas, A. Podestà and P. Milani, *PLOS ONE*, 2013, **8**, e68655.
22. H. M. H. Masuda and M. S. M. Satoh, *Japanese Journal of Applied Physics*, 1996, **35**, L126.
23. T. Yanagishita and H. Masuda, *Electrochimica Acta*, 2015, **184**, 80-85.
24. A. Christoulaki, C. Moretti, A. Chennevière, E. Dubois and N. Jouault, *Microporous and Mesoporous Materials*, 2020, **303**, 110201.
25. C. Lee, L. Joly, A. Siria, A.-L. Biance, R. Fulcrand and L. Bocquet, *Nano Letters*, 2012, **12**, 4037-4044.
26. J. O'sullivan and G. Wood, *Proceedings of the Royal Society of London. A. Mathematical and Physical Sciences*, 1970, **317**, 511-543.
27. I. Mínguez-Bacho, S. Rodríguez-López, A. Climent, D. Fichou, M. Vázquez and M. Hernández-Vélez, *The Journal of Physical Chemistry C*, 2015, **119**, 27392-27400.
28. I. Vrublevsky, K. Chernyakova, A. Ispas, A. Bund, N. Gaponik and A. Dubavik, *Journal of Luminescence*, 2011, **131**, 938-942.
29. H. Hashimoto, K. Yazawa, H. Asoh and S. Ono, *The Journal of Physical Chemistry C*, 2017, **121**, 12300-12307.
30. M. Baca, X. Carrier and J. Blanchard, *Chemistry – A European Journal*, 2008, **14**, 6142-6148.
31. M. L. Machesky and P. F. Jacobs, *Colloids and Surfaces*, 1991, **53**, 315-328.
32. G. Lefèvre, M. Duc, P. Lepeut, R. Caplain and M. Fédoroff, *Langmuir*, 2002, **18**, 7530-7537.
33. M. Engel, B. Stühn, J. J. Schneider, T. Cornelius and M. Naumann, *Applied Physics A*, 2009, **97**, 99-108.
34. T. Iijima, S. Kato, R. Ikeda, S. Ohki, G. Kido, M. Tansho and T. Shimizu, *Chemistry Letters*, 2005, **34**, 1286-1287.